Communication

Optimizing $K_{0.5}Na_{0.5}NbO_3$ Single Crystal by Engineering Piezoelectric Anisotropy

Weixiong Li [†] , **Chunxu Chen** [†] , **Guangzhong Xie and Yuanjie Su** *

State Key Laboratory of Electronic Thin Films and Integrated Devices, School of Optoelectronic Science and Engineering, University of Electronic Science and Technology of China (UESTC), Chengdu 610054, China; weixiong_li@std.uestc.edu.cn (W.L.); cxchen@std.uestc.edu.cn (C.C.); gzxie@uestc.edu.cn (G.X.)
* Correspondence: yjsu@uestc.edu.cn
† These authors contributed equally to the work.

Abstract: $K_{0.5}Na_{0.5}NbO_3$ is considered as one of the most promising lead-free piezoelectric ceramics in the field of wearable electronics because of its excellent piezoelectric properties and environmental friendliness. In this work, the temperature-dependent longitudinal piezoelectric coefficient d_{33}^* was investigated in $K_{0.5}Na_{0.5}NbO_3$ single crystals via the Landau–Ginzburg–Devonshire theory. Results show that the piezoelectric anisotropy varies with the temperature and the maximum of d_{33max}^* deviates from the polar direction of the ferroelectric phase. In the tetragonal phase, d_{33max}^{t*} parallels with cubic polarization direction near the tetragonal-cubic transition region, and then gradually switches toward the nonpolar direction with decreasing temperatures. The maximum of d_{33}^{o*} in the orthorhombic phase reveals a distinct varying trend in different crystal planes. As for the rhombohedral phase, slight fluctuation of the maximum of d_{33}^{r*} was observed and delivered a more stable temperature-dependent maximum d_{33max}^{r*} and its corresponding angle θ_{max} in comparison with tetragonal and orthorhombic phases. This work not only sheds some light on the temperature-dependent phase transitions, but also paves the way for the optimization of piezoelectric properties in piezoelectric materials and devices.

Keywords: piezoelectric; anisotropy; $K_{0.5}Na_{0.5}NbO_3$; phase; temperature

1. Introduction

With the gradual deepening and prosperity of the smart wearable industry revolution, piezoelectric-based flexible electronics have attracted considerable attention because of their promising applications in robotics [1], human–machine interaction (HMI) [2], energy harvesters [3], and internet of things (IOT) [4]. Lead-based perovskites, such as $Pb(Zr_xTi_{1−x})O_3$ (PZT) [5] and $Pb(Mg,Nb)O_3$ (PMN) [6] ceramics, possess huge piezoelectric properties but cause severe environmental and health concerns owing to their toxicity. As a promising alternative to lead zirconate titanate (PZT), the $K_{0.5}Na_{0.5}NbO_3$, a lead-free ferroelectric material, has exhibited outstanding piezoelectric performance near the polymorphic phase boundary (PPB) [7] and attracted massive attention worldwide in recent years due to its environmental friendliness [8–13]. Owing to its unique merits of a high piezoelectric coefficient (d_{33}), excellent ferroelectric properties, and a high Curie temperature (Tc = 420 °C), KNN has been widely utilized in energy-harvesting devices, transducers, actuators, and sensors [14–21]. Although pristine KNN ceramics possess relatively low piezoelectricity (d_{33}~80 pC/N), they can be remarkably improved by tuning sintering conditions [22], domain engineering [23], phase boundary engineering [24,25], texturing [26], and so on. Furthermore, since the intrinsic piezoelectric response is intimately associated with spontaneous polarization rotation, the anisotropy of piezoelectric capability plays a crucial role in the application of piezoelectric materials [27]. Anisotropy of piezoelectric properties had attracted massive attention in the 1980s, and unprecedented large piezoelectric anisotropy was observed in lead titanate ceramics with random grain

orientations [28,29]. However, limited works have focused on the piezoelectric anisotropy of $K_{0.5}Na_{0.5}NbO_3$ single crystals.

　　The main purpose of this work is to study the piezoelectric anisotropy of $K_{0.5}Na_{0.5}NbO_3$ single crystals as a function of temperature and to unravel the impact of phase transitions on the orientation and amplitude of the longitudinal piezoelectric coefficient. Landau–Ginzburg–Devonshire (LGD) theory was utilized to calculate the three-dimensional surface of the longitudinal piezoelectric coefficient d_{33}^* for KNN single crystals in three ferroelectric phases as a function of temperature. Temperature-dependent free energy and spontaneous polarization of KNN has also been investigated to interpret the derivation of piezoelectric coefficients stemmed from temperature variation.

2. Materials and Methods

　　The ferroelectric capabilities of KNN single crystals were systematically investigated through the Landau–Ginzburg–Devonshire (LGD) function. To achieve more convenience in expressing piezoelectric coefficients in light of the coordinate system for each ferroelectric phase, the cubic paraelectric phase was selected as the reference. The thermodynamic potential function G of the KNN single crystal can be written as [30,31]:

$$G(\sigma, E, T) = f_{LGD} + f_{elastic} + f_{electric} \tag{1}$$

where the Landau energy density is given by

$$
\begin{aligned}
f_{LGD} = {} & \alpha_1(P_1^2 + P_2^2 + P_3^2) + \alpha_{11}(P_1^4 + P_2^4 + P_3^4) + \alpha_{12}(P_1^2 P_2^2 + P_1^2 P_3^2 + P_2^2 P_3^2) \\
& + \alpha_{111}(P_1^6 + P_2^6 + P_3^6) + \alpha_{112}(P_1^2(P_2^4 + P_3^4) + P_2^2(P_3^4 + P_1^4) + P_3^2(P_1^4 + P_2^4)) \\
& + \alpha_{123}P_1^2 P_2^2 P_3^2 + \alpha_{1111}(P_1^8 + P_2^8 + P_3^8) + \alpha_{1122}(P_1^4 P_2^4 + P_1^4 P_3^4 + P_2^4 P_3^4) \\
& + \alpha_{1112}(P_1^6(P_2^2 + P_3^2) + P_2^6(P_3^2 + P_1^2) + P_3^6(P_1^2 + P_2^2)) \\
& + \alpha_{1123}(P_1^4 P_2^2 P_3^2 + P_2^4 P_3^2 P_1^2 + P_3^4 P_1^2 P_2^2) \\
& - \frac{1}{2}s_{11}(\sigma_1^2 + \sigma_2^2 + \sigma_3^2) - s_{12}(\sigma_1\sigma_2 + \sigma_1\sigma_3 + \sigma_2\sigma_3) \\
& - \frac{1}{2}s_{44}(\sigma_4^2 + \sigma_5^2 + \sigma_6^2) - Q_{11}(\sigma_1 P_1^2 + \sigma_2 P_2^2 + \sigma_3 P_3^2) \\
& - Q_{12}(\sigma_1(P_2^2 + P_3^2) + \sigma_2(P_3^2 + P_1^2) + \sigma_3(P_1^2 + P_2^2)) \\
& - Q_{44}(\sigma_4 P_2^2 P_3^3 + \sigma_5 P_1 P_3 + \sigma_6 P_1 P_2)
\end{aligned}
\tag{2}
$$

　　Here, α denotes the Landau coefficients determined under the stress-free condition [28], σ_i denotes the i_{th} component of stress in Voigt notation, s_{11}, s_{12}, and s_{44} denote the elastic compliance constants of a cubic phase [29–31], and Q_{11}, Q_{12}, and Q_{44} denote the corresponding electrostrictive coefficients between polarization and stress [32,33].

　　In this work, P_{ijP}^c, η_{ijP}^c, and d_{ijP}^c denote the polarization, dielectric susceptibility, and piezoelectric coefficient in the KNN single crystal for each phase, respectively. For studying the orientational dependence of piezoelectric coefficients, Euler angle (φ, θ, ψ) is utilized to quantitatively describe the rotation in terms of ferroelectric phase coordinates.

　　The Landau coefficients, elastic compliance constants, and electrostrictive coefficients are taken from Jianjun's previous work [34]. The dielectric constant possesses a positive proportional relationship with relative dielectric stiffness ($\varepsilon_{ij}^p = 1 + \eta_{ij}^p \approx \eta_{ij}^p$). $K_{0.5}Na_{0.5}NbO_3$ endures a series of phase transition (cubic→tetragonal→orthorhombic→rhombohedral) in the process of cooling from the paraelectric phase. The following relations were utilized to calculate the temperature-dependence of piezoelectric coefficients d_{ij}^p and dielectric susceptibility coefficients η_{ij}^p of KNN crystals as a function of spontaneous polarization,

$$\chi_{ij} = \varepsilon_0 \partial^2 f_{LGD} / \partial P_i \partial P_j (i, j = 1, 2, 3) \tag{3}$$
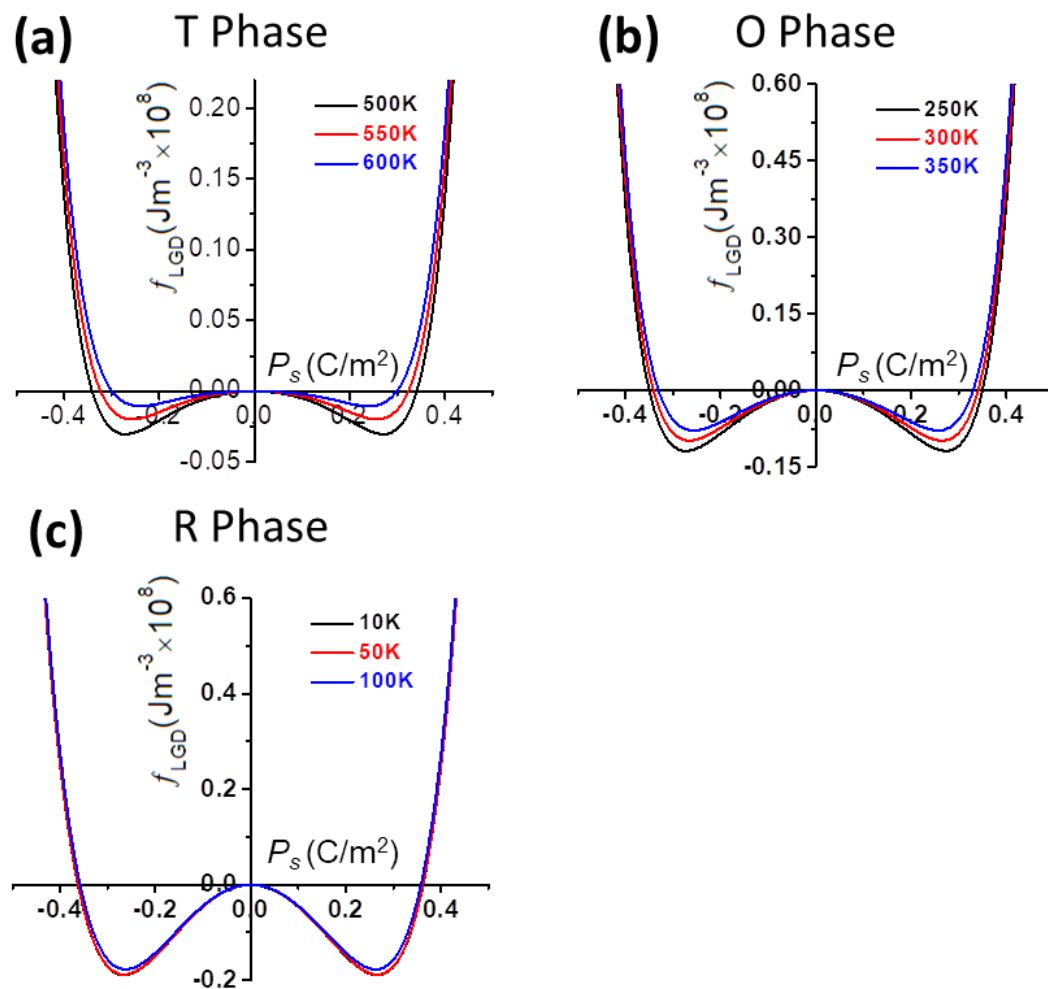
$$\eta_{ij} = A_{ji} / \Delta (i, j = 1, 2, 3) \tag{4}$$

$$g_{ij} = -\partial^2 f_{LGD}/\partial P_i \partial \sigma_j \tag{5}$$

$$d_{ij} = \varepsilon_0 \eta_{ik} g_{kj} \tag{6}$$

where A_{ji} and Δ refer to the cofactor and determinant of the χ_{ij} matrix.

3. Results and Discussion

The LGD-free energy density f_{LGD} of the tetragonal phase, orthorhombic phase, and rhombohedral phases, respectively, is plotted as a function of polarization at various temperatures, as shown in Figure 1a–c.

Figure 1. The Calculated LGD-free energy as a function of polarization (Ps) in (**a**) tetragonal phase, (**b**) orthorhombic phase, (**c**) rhombohedral phase at various temperatures.

Figures 2 and 3, respectively, elucidate the calculated dielectric susceptibility coefficients η_{ij}^{p} and piezoelectric coefficients d_{ij}^{p} for $K_{0.5}Na_{0.5}NbO_3$ single crystals as a function of temperature in all three ferroelectric phases, respectively.
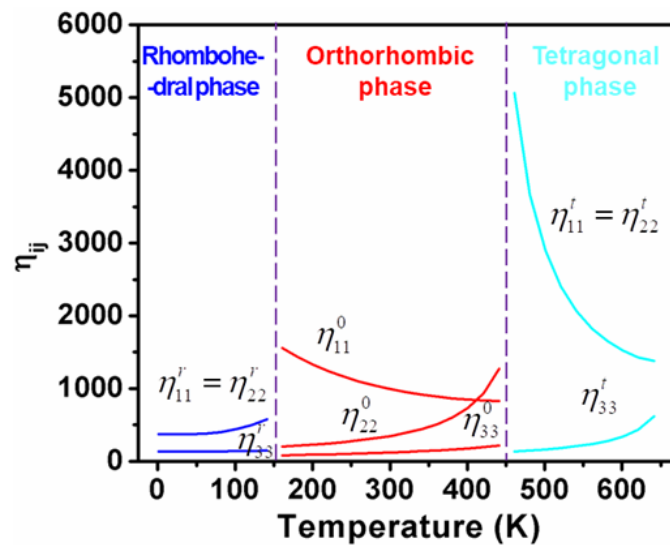
Figure 2. Calculated dielectric susceptibility coefficients for $K_{0.5}Na_{0.5}NbO_3$ single crystals as functions of temperature in all three ferroelectric phases.
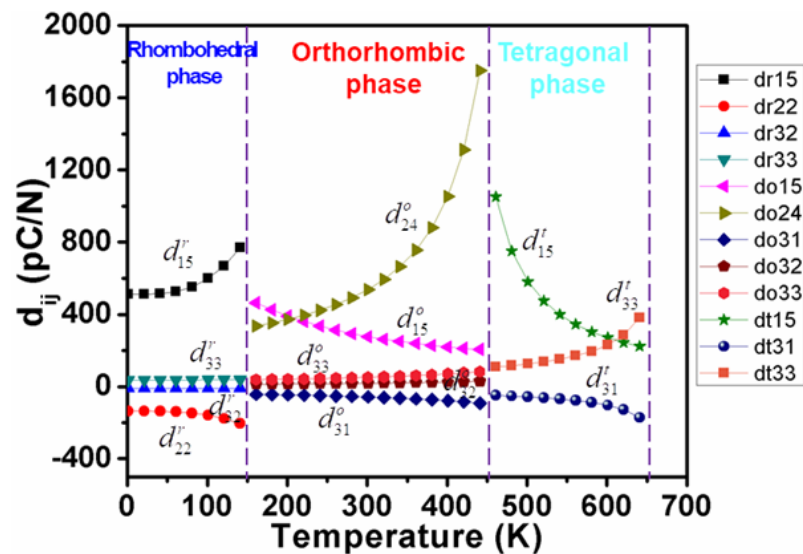

Figure 3. Calculated piezoelectric coefficients for $K_{0.5}Na_{0.5}NbO_3$ single crystals as functions of temperature in all three ferroelectric phases.

According to the Landau–Ginsburg–Devonshire theory, the polarization, i.e., the second derivative of thermodynamic potential function G, can be acquired as a function of temperature by minimizing the total free energy in terms of polarization. Figure 4 illustrates the temperature-dependent spontaneous polarization of $K_{0.5}Na_{0.5}NbO_3$ single crystals in the three phases. It can be clearly seen that polarization goes up with the cooling process for all the ferroelectric phases. Sudden rises were observed at the regions of phase transitions, where 648 K for cubic to tetragonal, 469 K for tetragonal to orthorhombic, and 130 K for orthorhombic to rhombohedral, which is consistent with the experimental results of 694 K, 468 K and 125 K, respectively, from Egerton et al. [35]. It is worth noting that the calculated polarization becomes zero when the temperature is approaching Curie temperature, implying that the system switches to paraelectric phase. Figure 5 displays the free energy (ΔG) of $K_{0.5}Na_{0.5}NbO_3$ single crystals in the three phases as a function of temperatures.
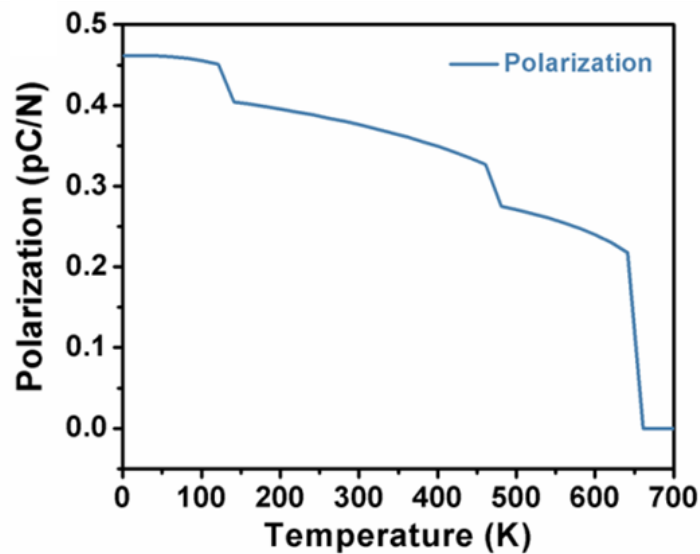
Figure 4. Spontaneous polarization of $K_{0.5}Na_{0.5}NbO_3$ single crystals as a function of temperatures.
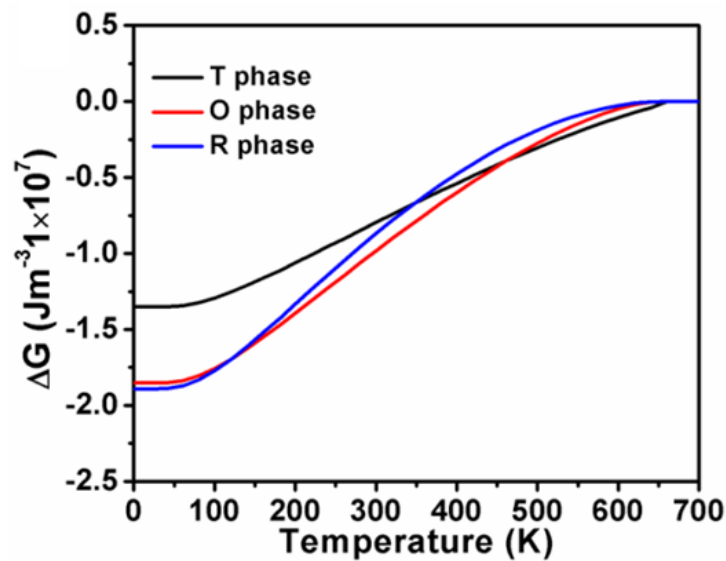

Figure 5. Free energy (ΔG) of $K_{0.5}Na_{0.5}NbO_3$ single crystals in the three phases as a function of temperatures.
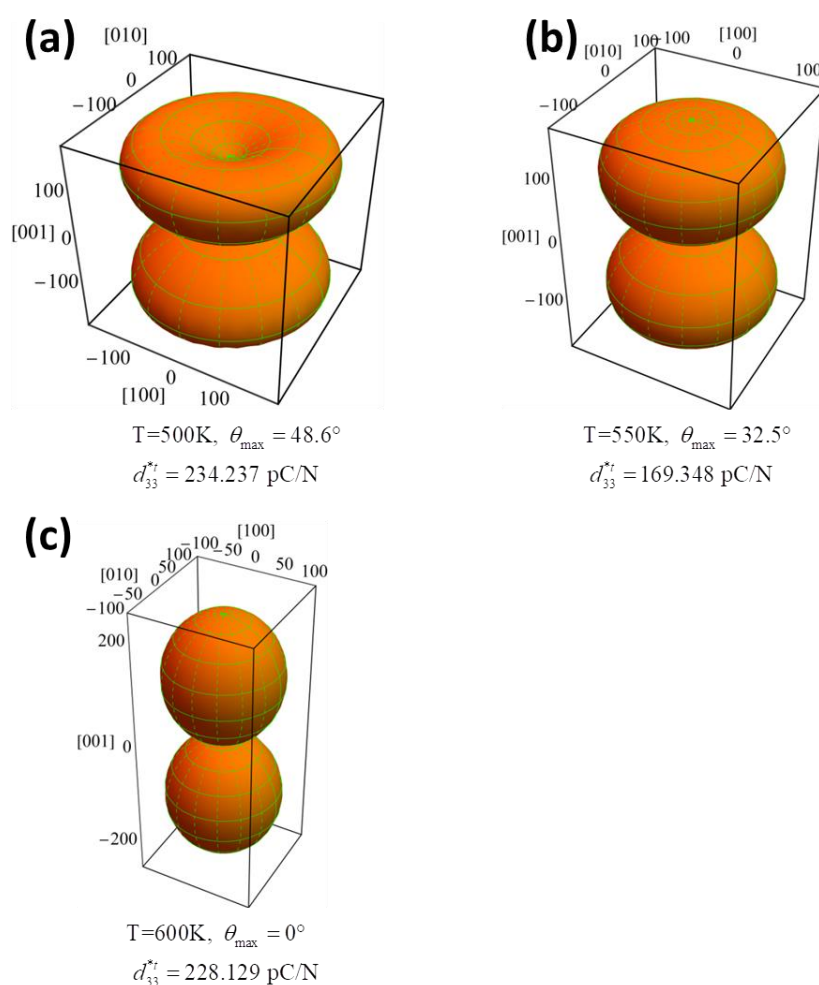
The piezoelectric properties are proportional to the flattening of the free energy profile. It can be clearly seen that the tetragonal-cubic phase transition causing an enhanced d^t_{33} (Figure 3) can also be explained by the flattening of the free energy profile (Figure 1a). Consequently, the delayering of the free energy profile favors the enhancement of dielectric susceptibility. It is obvious that in the orthorhombic phase, the increasing temperature flattens the LGD-free energy well and makes it shallower with the heating-up process (Figure 1b), giving rise to the increase in dielectric susceptibility, and thus the increase in its piezoelectric response (Figure 1b). As for the temperature-dependent free energy for the rhombohedral phase in Figure 1c, the delayering of the free energy arising from the temperature rising also contributes to the enhancement of piezoelectric coefficients lying along a no-polar direction (Figure 3).

In the tetragonal phase, the value of d_{33}^t for $K_{0.5}Na_{0.5}NbO_3$ crystals in the rotated coordinate along an arbitrary direction can be expressed as:

$$d_{33}^{t*}(\theta) = \cos\theta(d_{15}^t \sin^2\theta + d_{31}^t \sin^2\theta + d_{33}^t \cos^2\theta) \qquad (7)$$

where angle θ denotes rotation always from $[100]^t$. In the tetragonal phase, ($P_1 = P_2 = 0$, $P_3 = P_{3T}^c \neq 0$).

Therefore, by using Equation (7), the three-dimensional profile of calculated $d_{33}^{t*}(\theta)$ of the tetragonal phase for three selected temperatures 500, 550, and 600 K is displayed in Figure 6a–c, respectively. As the temperature goes down from the cubic phase to the orthorhombic phase, the surface of $d_{33}^{t*}(\theta)$ varies during the cooling process. The direction of the largest $d_{33max}^{t*}(\theta)$ lies along $[001]_c$ direction at 600 K then switches to $\theta_{max} = 32.5°$ at 550 K, and finally to $\theta_{max} = 48.6°$ at 500 K.

T=500K, $\theta_{max} = 48.6°$
$d_{33}^{*t} = 234.237$ pC/N

T=550K, $\theta_{max} = 32.5°$
$d_{33}^{*t} = 169.348$ pC/N

T=600K, $\theta_{max} = 0°$
$d_{33}^{*t} = 228.129$ pC/N

Figure 6. The orientation dependence of piezoelectric coefficient of $K_{0.5}Na_{0.5}NbO_3$ single crystals in the tetragonal phases at the temperature of (**a**) 500 K, (**b**) 550 K, (**c**) 600 K.

Attributed to the expression of $d_{33}^{t*}(\theta)$ in Equation (7), it is obvious that $d_{33}^{t*}(\theta)$ is determined by three parameters d_{33}^t, d_{31}^t, and d_{15}^t.

As shown in Figure 3, d_{33}^t and d_{15}^t changes rapidly near the temperature range of tetragonal-cubic and tetragonal-orthorhombic phase transitions, respectively, while little change in d_{31}^t was observed in comparison with d_{33}^t and d_{15}^t. The d_{15}^t behaves like the dielectric permittivity (η_{11}^t, η_{22}^t) in the cubic phase as a function of temperature and increases

with the process of cooling down toward the ferroelectric phase. When the temperature rises toward to the cubic phase (Figure 3), d_{33}^t surpasses d_{15}^t obviously.

As shown in Figure 2, calculated dielectric constants η_{11}^t and η_{33}^t vary in opposite tendencies in the whole tetragonal phase temperature range, which gives rise to a maximum $d_{33max}^{t*}(\theta)$ along the polar direction in the high-temperature range. As displayed in Figures 7 and 8, the corresponding angle θ for the maximum value of d_{33}^{t*} varies as a function of temperatures, which clearly demonstrates the influence of temperature on the phase transition. It can be seen that the maximum $d_{33max}^{t*}(\theta)$ stays along $[001]^t$ at high temperatures but deviates from $[001]^t$ to the nonpolar direction when the temperature goes down, near the orthorhombic-tetragonal point. At the temperature T = 450 K, the maximum $d_{33max}^{t*}(\theta)$ = 521.9 pC/N lies along the direction defined by θ_{max} = 52.98°. The maximum $d_{33max}^{t*}(\theta)$ decreases at first, and then rises with increasing temperature, leading to a minimum at 550 K. This is because d_{15}^t keeps increasing while $d_{33}^{t*}(\theta)$ keeps decreasing during the cooling process, leading to the orientation variation and amplitude change of maximum $d_{33max}^{t*}(\theta)$. It is reported that the pure KNN at 433 K exhibits a piezoelectric coefficient of 108 pC/N [36], which is similar to our calculated results (Figure 7) along the polar direction at 500 K. As shown in Figure 8, the angle θ_{max} for the maximum $d_{33max}^{t*}(\theta)$ in tetragonal $K_{0.5}Na_{0.5}NbO_3$ deviates away from 0° once the temperature is below 560 K. It should be noted that the $d_{33max}^{t*}(\theta)$ of $KNbO_3$ (KNO) single crystals follows a similar tendency as that for the KNN single crystal because they have the same phase transition sequences and structures [37]. As for the $PbTiO_3$ single crystal [38], the maximum $d_{33max}^{t*}(\theta)$ lies along the polar direction at all temperatures because its shear coefficient is too small at all temperatures to rotate d_{33} away from the polar direction, which is quite different from the change trend for KNN.
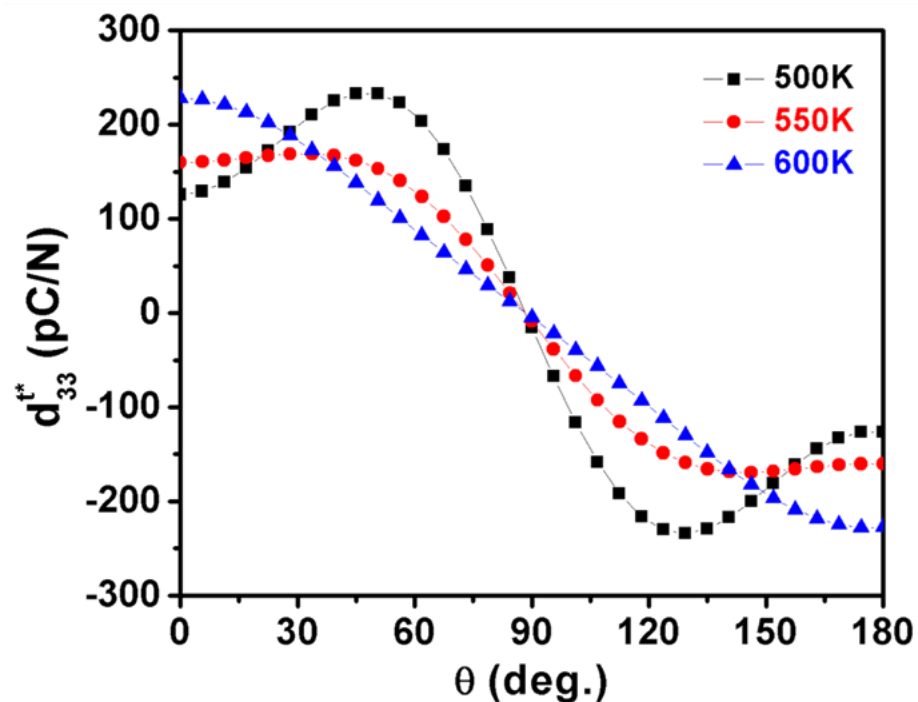

Figure 7. The piezoelectric coefficient in the tetragonal $K_{0.5}Na_{0.5}NbO_3$ as a function of angle θ at various temperatures.
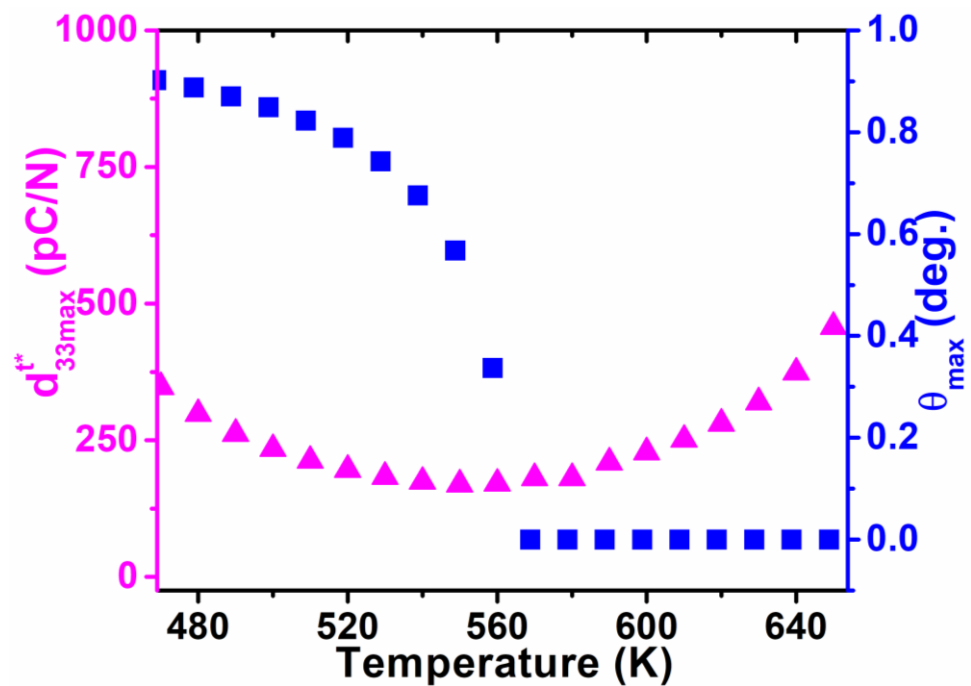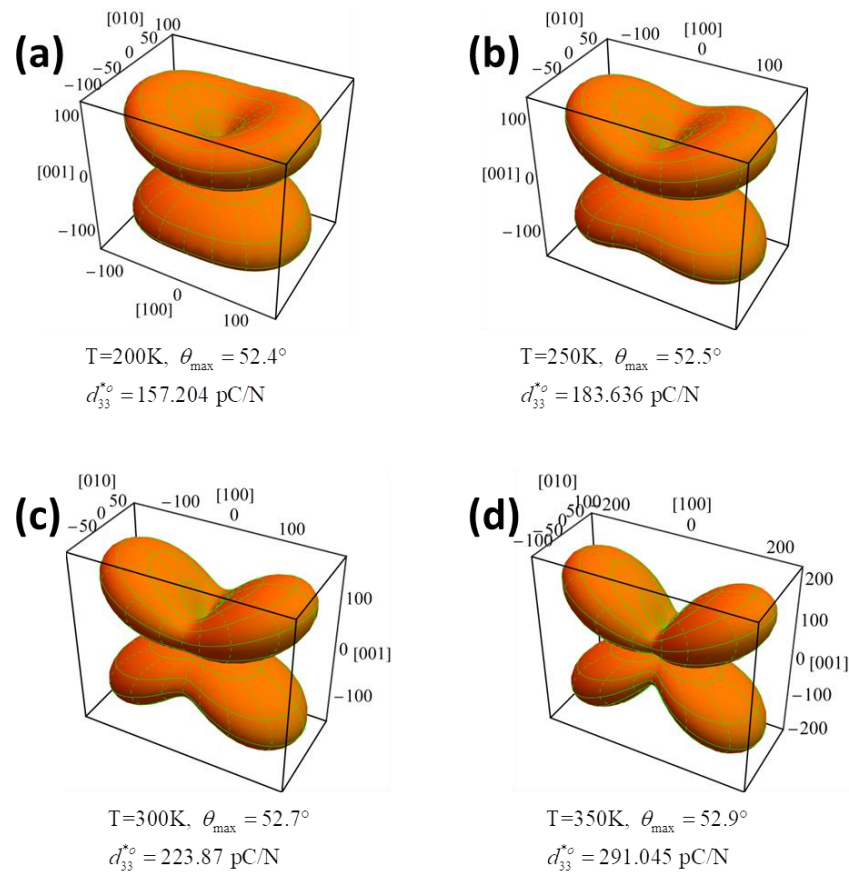
Figure 8. Maximum of piezoelectric coefficient and its corresponding angle θ_{max} as a function of temperature for the tetragonal $K_{0.5}Na_{0.5}NbO_3$.

In the orthorhombic phase, more complex behaviors were observed in the variation of piezoelectric coefficients as a function of temperature in $K_{0.5}Na_{0.5}NbO_3$ (Figure 3). Compared with d_{31}^o, d_{32}^o, and d_{33}^o that are relatively insensitive to temperature, the two different shear coefficients play a key role in piezoelectricity, where the shear piezoelectric coefficient d_{15}^o declines with increasing temperature, while d_{24}^o follows an opposite tendency, as shown in Figure 3. As a consequence, the piezoelectric coefficient d_{33}^{o*} in $K_{0.5}Na_{0.5}NbO_3$ exhibits a more sophisticated temperature-dependent trend compared with the tetragonal phase:

$$d_{33}^{o*}(\phi, \theta) = \cos\theta[(d_{15}^o + d_{31}^o)\sin^2\theta\sin^2\phi + (d_{24}^o + d_{32}^o)\sin^2\theta\cos^2\phi + d_{33}^o\cos^2\theta)] \quad (8)$$

For the orthorhombic phase with $P_1 = 0$, $P_2 = P_3 = P_{3O}^c \neq 0$, the surface of the piezoelectric coefficient at four chosen temperatures of 200 K, 250 K, 300 K, and 350 K are respectively shown in Figure 9a–d. With a decreasing temperature, the direction of the maximum d_{33}^{o*} was slightly changed from the polar direction [001]°. The distinct changing tendencies of d_{15}^o and d_{24}^o are apparently responsible for the 90° rotation of the direction of the maximum d_{33}^{o*} in the cooling process. For instance, at 200 K, the maximum d_{33}^{o*} of 157.204 pC/N lies along the direction defined by $\theta = 52.4°$ and $\varphi = \pi/2$ (Figure 9a), but switches to the direction defined by $\theta = 52.9°$ and $\varphi = 0$ at 350 K with an amplitude of 291 pC/N (Figure 9d). Note that the d_{33}^{o*} reaches up to 223.87 pC/N at 300 K, which is very closed to the experimental results of 218 pC/N, indicating the accuracy and reliability of our modeling and calculation [39].

(a) T=200K, $\theta_{max} = 52.4°$
$d_{33}^{*o} = 157.204$ pC/N

(b) T=250K, $\theta_{max} = 52.5°$
$d_{33}^{*o} = 183.636$ pC/N

(c) T=300K, $\theta_{max} = 52.7°$
$d_{33}^{*o} = 223.87$ pC/N

(d) T=350K, $\theta_{max} = 52.9°$
$d_{33}^{*o} = 291.045$ pC/N

Figure 9. The orientation dependence of piezoelectric coefficient of $K_{0.5}Na_{0.5}NbO_3$ single crystals in the orthorhombic phases at the temperature of (**a**) 200 K, (**b**) 250 K, (**c**) 300 K, (**d**) 350 K.

As unraveled in Figures 10–13, the temperature-dependent maximum d_{33max}^{o*} and its corresponding angle θ_{max} are illustrated in planes of $\varphi = 0$ and $\varphi = \pi/2$ to systematically indicate the piezoelectric anisotropy of the orthorhombic $K_{0.5}Na_{0.5}NbO_3$, where the direction of the maximum d_{33max}^{o*} is rotated by 90° with an increasing temperature, and its amplitude attains the largest value in the high-temperature range when approaching the tetragonal phase.
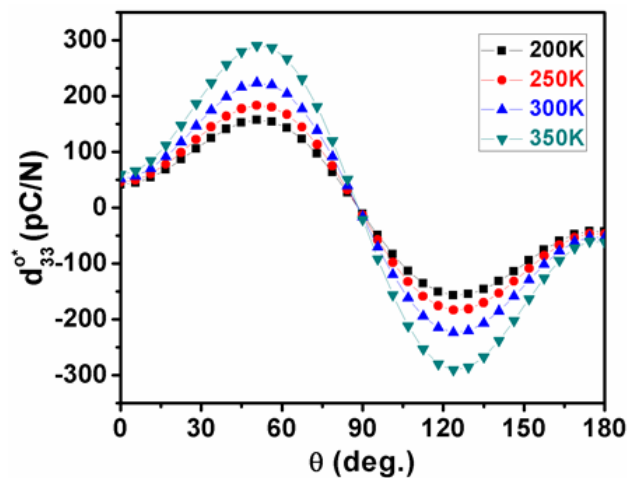
Figure 10. The piezoelectric coefficient in the orthorhombic $K_{0.5}Na_{0.5}NbO_3$ as a function of angle θ under various temperatures in planes of $\varphi = 0$.
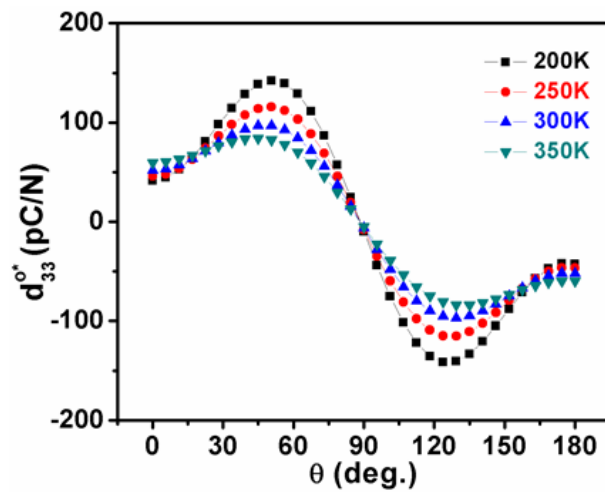
Figure 11. The piezoelectric coefficient in the orthorhombic $K_{0.5}Na_{0.5}NbO_3$ as a function of angle θ under various temperatures in planes of $\varphi = \pi/2$.
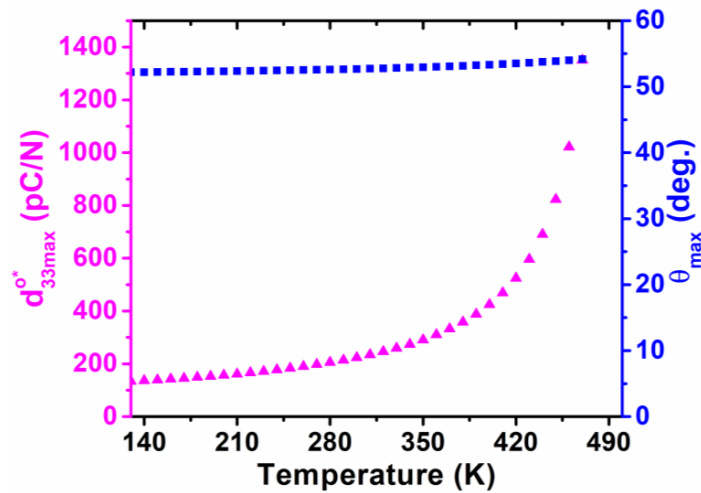

Figure 12. Maximum of piezoelectric coefficient and its corresponding angle θ_{max} as a function of temperature for the orthorhombic $K_{0.5}Na_{0.5}NbO_3$ in planes of $\varphi = 0$.
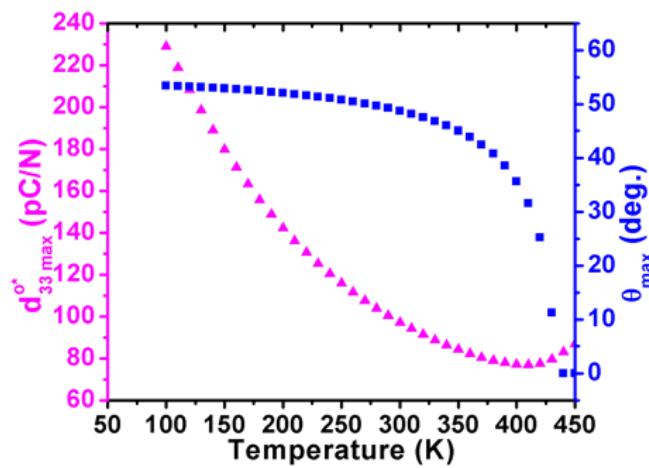

Figure 13. Maximum of piezoelectric coefficient and its corresponding angle θ_{max} as a function of temperature for the orthorhombic $K_{0.5}Na_{0.5}NbO_3$ in planes of $\varphi = \pi/2$.

According to the calculated LGD-free energy-polarization relationship as plotted in Figure 1b, the flattening of the LGD-free energy well arising from temperature growth enhances dielectric susceptibility, as well as piezoelectric response. This tendency further endows stronger effects on the piezoelectric response of KNN single crystals in the tetragonal-orthorhombic transition instead of the orthorhombic-rhombohedral transition.

As for the low-temperature rhombohedral phase, the orientation dependence of d_{33}^{r*} can be given by

$$d_{33}^{r*}(\theta, \psi) = d_{15}^r \cos\theta \sin^2\theta - d_{22}^r \sin^3\theta + d_{31}^r \sin^2\theta \cos\theta + d_{33}^r \cos^3\theta \qquad (9)$$

As displayed in Figure 14a–c, similar three-dimensional surfaces of d_{33}^{r*} were observed at temperatures of 50 K, 75 K and 100 K, implying that the temperature variation in the rhombohedral phase causes less impact on the three-dimensional surface of d_{33}^{r*} in comparison with those for the tetragonal and orthorhombic phase. Since no lower-symmetry phase exists as the temperature is approaching toward 0 K, the rhombohedral phase is the most stable one, and the three-dimensional surface of d_{33}^{r*} remains unchanged when the K$_{0.5}$Na$_{0.5}$NbO$_3$ single crystal was gradually frozen during the cooling process.
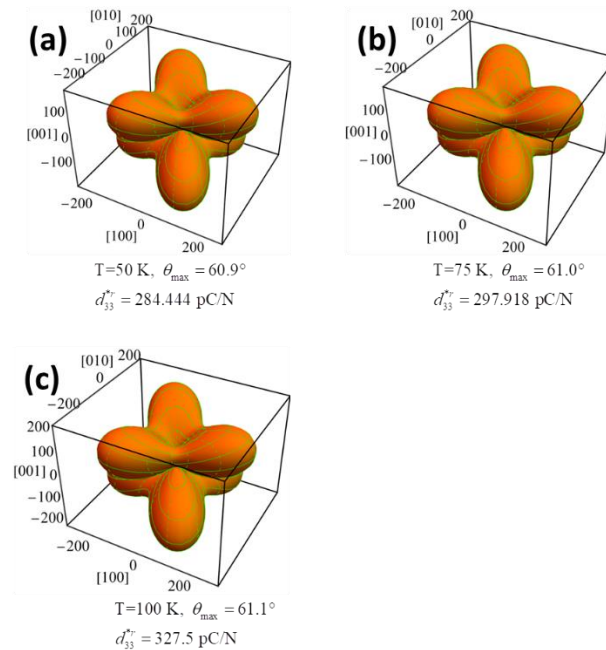

Figure 14. The orientation dependence of coefficient of K$_{0.5}$Na$_{0.5}$NbO$_3$ single crystals in the rhombohedral phases at the temperature of (**a**) 50 K, (**b**) 75 K, (**c**) 100 K.

It is found that d_{15}^r, d_{22}^r (negative value) are proportional to the temperature, while d_{32}^r and d_{33}^r are almost temperature independent in the rhombohedral phase (Figure 3). As a result, the three-dimensional surface of d_{33}^r slightly varies with varying temperatures, as shown in Figure 14a–c. At 50 K, the maximum d_{33}^{r*} of 284.444 pC/N lies along the direction defined by $\theta = 60.9°$ and $\varphi = 0$ (Figure 14a), while at 100 K, the maximum d_{33}^{r*} switches to the direction defined by $\theta = 61.1°$ and $\varphi = 0$ with an amplitude of 327.5 pC/N (Figure 14c). The dependence of the piezoelectric coefficient d_{33}^{r*} in KNN on the θ under various temperatures is revealed in Figure 15. The direction of the maximum value of d_{33}^{r*} varies with rising temperatures from 0 K to 130 K in the rhombohedral phase (Figure 16). Both maximum d_{33max}^{r*} and its corresponding angle θ_{max} are proportional to the temperature. The angles θ are higher than $\theta = 54.73°$, which is consistent with the [001]^c (or [111]$_r$) direction.
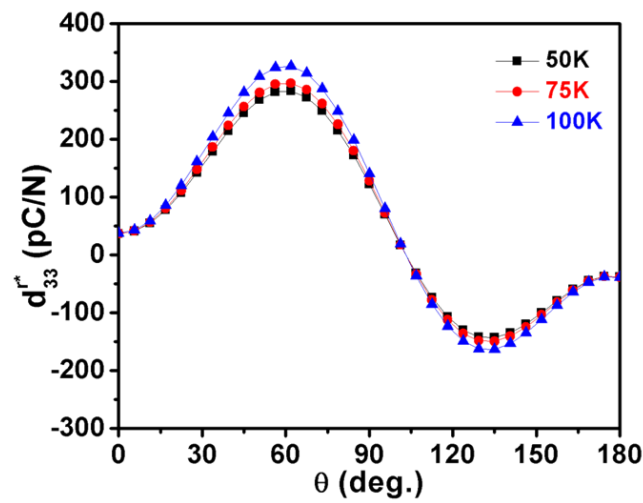
Figure 15. The piezoelectric coefficient in the rhombohedral $K_{0.5}Na_{0.5}NbO_3$ as a function of angle θ at various temperatures.
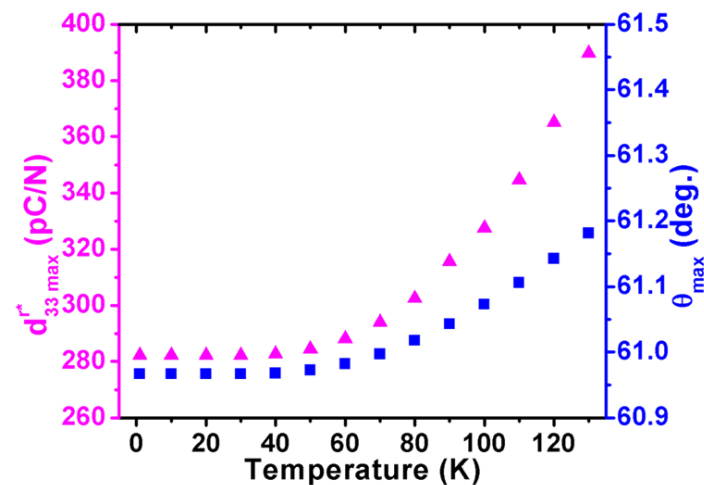
Figure 16. Maximum and its corresponding angle θ_{max} as a function of temperature for the rhombohedral $K_{0.5}Na_{0.5}NbO_3$.

According to the expression of d_{33}^{r*} in Equation (9), d_{33}^{r*} reveals an asymmetry attribute with respect to the axis defined by $\theta = 90°$. It is obvious that the enhanced dielectric susceptibility, which is perpendicular to the polar direction, renders the large change in d_{15}^r. The polarization rotation near the phase transition region gives rise to the increase of piezoelectric response upon the heating process, which brings about the rotation of the maximum d_{33max}^{r*} and the slight variation in d_{33}^r. Furthermore, with respect to the LGD-free energy profile (Figure 1c), the delayering of the free energy well with increasing temperatures indicates that the piezoelectric coefficients enhance toward a no-polar direction.

4. Conclusions

In summary, LGD thermodynamic theory was utilized to investigate the temperature-induced phase transition and evolution of three-dimensional d_{33}^* surface in KNN single crystals. The dielectric softening along the direction perpendicular to the polarization axis is responsible for the direction change of the maximum d_{33}^* under various temperatures. During the ferroelectric phase transition, the increase of shear piezoelectric coefficients renders a significant enhancement in d_{33}^* along the non-polar direction. This work not only looks into the fundamental understanding of the temperature-dependent phase transitions,

but also paves the way for the optimization of piezoelectric properties in ferroelectric materials.

References

1. Han, M.; Wang, H.; Yang, Y.; Liang, C.; Bai, W.; Yan, Z.; Li, H.; Xue, Y.; Wang, X.; Akar, B.; et al. Three-dimensional piezoelectric polymer microsystems for vibrational energy harvesting, robotic interfaces and biomedical implants. *Nat. Electron.* **2019**, *2*, 26–35. [CrossRef]
2. Lim, S.; Son, D.; Kim, J.; Lee, Y.B.; Song, J.K.; Choi, S.; Lee, D.J.; Kim, J.H.; Lee, M.; Hyeon, T.; et al. Transparent and Stretchable Interactive Human Machine Interface Based on Patterned Graphene Heterostructures. *Adv. Funct. Mater.* **2015**, *25*, 375–383. [CrossRef]
3. Wang, X.; Song, J.; Liu, J.; Wang, Z.L. Direct-Current Nanogenerator Driven by Ultrasonic Waves. *Science* **2007**, *316*, 102–105. [CrossRef] [PubMed]
4. Chorsi, M.T.; Curry, E.J.; Chorsi, H.T.; Das, R.; Baroody, J.; Purohit, P.K.; Ilies, H.; Nguyen, T.D. Piezoelectric biomaterials for sensors and actuators. *Adv. Mater.* **2019**, *31*, 1802084. [CrossRef] [PubMed]
5. Deng, Y.; Wang, J.L.; Zhu, K.R.; Zhang, M.S.; Hong, J.M.; Gu, Q.R.; Yin, Z. Synthesis and characterization of single-crystal $PbTiO_3$ nanorods. *Mater. Lett.* **2005**, *59*, 3272–3275. [CrossRef]
6. Li, F.; Cabral, M.J.; Xu, B.; Cheng, Z.; Dickey, E.C.; LeBeau, J.M.; Wang, J.L.; Luo, J.; Taylor, S.; Hackenberger, W.; et al. Giant piezoelectricity of Sm-doped $Pb(Mg_{1/3}Nb_{2/3})O_3$-$PbTiO_3$ single crystals. *Science* **2019**, *364*, 264–268. [CrossRef]
7. Wang, K.; Malič, B.; Wu, J. Shifting the phase boundary: Potassium sodium niobate derivates. *MRS Bull.* **2018**, *43*, 607–611. [CrossRef]
8. Helden, L.; Bogula, L.; Janolin, P.; Hanke, M.; Breuer, T.; Schmidbauer, M.; Ganschow, S.; Schwarzkopf, J. Huge impact of compressive strain on phase transition temperatures in epitaxial ferroelectric $KxNa1-xNbO_3$ thin films. *Appl. Phys. Lett.* **2019**, *114*, 232905. [CrossRef]
9. Schmidbauer, M.; Braun, D.; Markurt, T.; Hanke, M.; Schwarzkopf, J. Strain engineering of monoclinic domains in $K_xNa_{1-x}NbO_3$ epitaxial layers: A pathway to enhanced piezoelectric properties. *Nanotechnology* **2017**, *28*, 24LT02. [CrossRef]
10. Wang, K.; Li, J.F. Domain Engineering of Lead-Free Li-Modified $(K, Na)NbO_3$ Polycrystals with Highly Enhanced Piezoelectricity. *Adv. Funct. Mater.* **2010**, *20*, 1924–1929. [CrossRef]
11. Hollenstein, E.; Davis, M.; Damjanovic, D.; Setter, N. Piezoelectric properties of Li- and Ta-modified $(K_{0.5}Na_{0.5})NbO_3$ ceramics. *Appl. Phys. Lett.* **2005**, *87*, 82905. [CrossRef]
12. Matsubara, M.; Kikuta, K.; Hirano, S. Piezoelectric properties of $(K_{0.5}Na_{0.5})(Nb_{1-x}Ta_x)O_3-K_{5.4}CuTa_{10}O_{29}$ ceramics. *J. Appl. Phys.* **2005**, *97*, 114105. [CrossRef]
13. Mgbemere, H.E.; Hinterstein, M.; Schneider, G.A. Structural phase transitions and electrical properties of $(K_xNa_{1-x})NbO_3$-based ceramics modified with Mn. *J. Eur. Ceram. Soc.* **2012**, *32*, 4341–4352. [CrossRef]
14. Shirane, G.; Newnham, R.; Pepinsky, R. Dielectric Properties and Phase Transitions of $NaNbO_3$ and $(Na,K)NbO_3$. *Phys. Rev.* **1954**, *96*, 581. [CrossRef]
15. Jiang, M.; Zhang, J.; Rao, G.; Li, D.; Randall, C.A.; Li, T.; Peng, B.; Li, L.; Gu, Z.; Liu, X.; et al. Ultrahigh piezoelectric coefficient of a lead-free $K_{0.5}Na_{0.5}NbO_3$-based single crystal fabricated by a simple seed-free solid-state growth method. *J. Mater. Chem. C* **2019**, *7*, 14816–14844. [CrossRef]
16. Liu, H.; Veber, P.; Rödel, J.; Rytz, D.; Fabritchnyi, P.B.; Afanasov, M.I.; Patterson, E.A.; Frömling, T.; Maglione, M.; Koruza, J. High-performance piezoelectric $(K,Na,Li)(Nb,Ta,Sb)O_3$ single crystals by oxygen annealing. *Acta Mater.* **2018**, *148*, 499–507. [CrossRef]
17. Zhu, B.; Zhu, Y.; Yang, J.; Ou-Yang, J.; Yang, X.; Li, Y.; Wei, W. New Potassium Sodium Niobate Single Crystal with Thickness-independent High-performance for Photoacoustic Angiography of Atherosclerotic Lesion. *Sci. Rep.* **2016**, *6*, 39679. [CrossRef] [PubMed]

18. Ma, J.; Xue, S.; Zhao, X.; Wang, F.; Tang, Y.; Duan, Z.; Wang, T.; Shi, W.; Yue, Q.; Zhou, H.; et al. High frequency transducer for vessel imaging based on lead-free Mn-doped ($K_{0.44}Na_{0.56}$)NbO_3 single crystal. *Appl. Phys. Lett.* **2017**, *111*, 092903. [CrossRef]

19. Koruza, J.; Liu, H.; Höfling, M.; Zhang, M.-H.; Veber, P. (K,Na)NbO_3-based piezoelectric single crystals: Growth methods, properties, and applications. *J. Mater. Res.* **2020**, *35*, 990–1016. [CrossRef]

20. Rodel, J.; Li, J.-F. Lead-free piezoceramics: Status and perspectives. *MRS Bull.* **2018**, *43*, 576–580. [CrossRef]

21. Li, J.F.; Wang, K.; Zhu, F.Y.; Cheng, L.Q.; Yao, F.Z. (K,Na)NbO_3-Based Lead-Free Piezoceramics: Fundamental Aspects, Processing Technologies, and Remaining Challenges. *J. Am. Ceram. Soc.* **2013**, *96*, 3677–3696. [CrossRef]

22. Li, J.-F.; Wang, K.; Zhang, B.-P.; Zhang, L.-M. Ferroelectric and Piezoelectric Properties of Fine-Grained $Na_{0.5}K_{0.5}NbO_3$ Lead-Free Piezoelectric Ceramics Prepared by Spark Plasma Sintering. *J. Am. Ceram. Soc.* **2006**, *89*, 706–709. [CrossRef]

23. Yao, F.; Wang, K.; Cheng, L.; Zhang, X.; Zhang, W.; Zhu, F.; Li, J. Nanodomain Engineered (K,Na)NbO_3 Lead-Free Piezoceramics: Enhanced Thermal and Cycling Reliabilities. *J. Am. Ceram. Soc.* **2015**, *98*, 448–454. [CrossRef]

24. Lv, X.; Zhang, J.; Liu, Y.; Li, F.; Zhang, X.; Wu, J. Synergetic Contributions in Phase Boundary Engineering to the Piezoelectricity of Potassium Sodium Niobate Lead-Free Piezoceramics. *ACS Appl. Mater. Interfaces* **2020**, *12*, 39455–39461. [CrossRef]

25. Wu, J.; Xiao, D.; Zhu, J. Potassium–sodium niobate lead-free piezoelectric materials: Past, present, and future of phase boundaries. *Chem. Rev.* **2015**, *115*, 2559–2595. [CrossRef]

26. Li, P.; Zhai, J.; Shen, B.; Zhang, S.; Li, X.; Zhu, F.; Zhang, X. Ultrahigh piezoelectric properties in textured (K, Na) NbO_3-based lead-free ceramics. *Adv. Mater.* **2018**, *30*, 1705171. [CrossRef]

27. Uchino, K.; OH, K. Piezoelectric anisotropy and polarization sublattice coupling in perovskite crystals. *J. Am. Ceram. Soc.* **1991**, *74*, 1131–1134. [CrossRef]

28. Takeuchi, H.; Jyomura, S.; Yamamoto, E.; Ito, Y. Electromechanical properties of (Pb, Ln) (Ti, Mn) O_3 ceramics (Ln= rare earths). *J. Acoust. Soc. Am.* **1982**, *72*, 1114–1120. [CrossRef]

29. Newnham, K.; Skinner, D.; Cross, L. Connectivity and piezoelectric-pyroelectric composites. *Mat. Res. Bull.* **1978**, *13*, 525–536. [CrossRef]

30. Damjanovic, D. Ferroelectric, dielectric and piezoelectric properties of ferroelectric thin films and ceramics. *Rep. Prog. Phys.* **1998**, *61*, 1267. [CrossRef]

31. Pohlmann, H.; Wang, J.; Wang, B.; Chen, L. A thermodynamic potential and the temperature-composition phase diagram for single-crystalline $K_{1-x}Na_xNbO_3$ ($0 \leq x \leq 0.5$). *Appl. Phys. Lett.* **2017**, *110*, 102906. [CrossRef]

32. Wang, B.; Chen, N.; Wang, J.; Chen, L. Ferroelectric domain structures and temperature-misfit strain phase diagrams of $K_{1-x}Na_xNbO_3$ thin films: A phase-field study. *Appl. Phys. Lett.* **2019**, *115*, 092902. [CrossRef]

33. Cao, G.; Huang, H.; Liang, D.; Ma, X. A phenomenological potential and ferroelectric properties of $BaTiO_3$–$CaTiO_3$ solid solution. *Ceram. Int.* **2017**, *43*, 6671–6676. [CrossRef]

34. Zhou, M.; Wang, J.; Chen, L.; Nan, C. Strain, temperature, and electric-field effects on the phase transition and piezoelectric responses of $K_{0.5}Na_{0.5}NbO_3$ thin films. *J. Appl. Phys.* **2018**, *123*, 154106. [CrossRef]

35. Tagantsev, A.K. Landau Expansion for Ferroelectrics: Which Variable to Use? *Ferroelectrics* **2008**, *375*, 19–27. [CrossRef]

36. Li, L.; Gong, Y.; Gong, L.; Dong, H.; Yi, X.; Zheng, X. Low-temperature hydro/solvothermal synthesis of Ta-modified K0.5Na0.5NbO powders and piezoelectric properties of corresponding ceramics. *Mater. Des.* **2012**, *33*, 362–366. [CrossRef]

37. Liang, L.; Li, Y.; Hu, S.; Chen, L.; Lu, G. Piezoelectric anisotropy of a $KNbO_3$ single crystal. *J. Appl. Phys.* **2010**, *108*, 094111. [CrossRef]

38. Budimir, M.; Damjanovic, D.; Setter, N. Piezoelectric anisotropy–phase transition relations in perovskite single crystals. *J. Appl. Phys.* **2003**, *94*, 6753–6761. [CrossRef]

39. Long, C.; Li, T.; Fan, H.; Wu, Y.; Zhou, L.; Li, Y.; Xiao, L.; Li, Y. Li-substituted $K_{0.5}Na_{0.5}NbO_3$-based piezoelectric ceramics: Crystalstructures and the effect of atmosphere on electrical properties. *J. Alloy. Compd.* **2016**, *658*, 839–847. [CrossRef]